

## Supporting Information

# Mass Production of Nitrogen and Oxygen Codoped Carbon Nanotubes by a Delicate-Designed Pechini Method for Supercapacitor and Electrocatalysis

Shuai Qi,<sup>a</sup> Dong Wang,<sup>\* a</sup> Weijian Li,<sup>b</sup> Rui Zhang,<sup>c</sup> Feng Liu,<sup>a</sup> Juntao Zhang,<sup>a</sup> Zhiyuan Liu,<sup>a</sup>  
Yana Guo,<sup>a</sup> Fagang Wang,<sup>\* a</sup> and Guangwu Wen<sup>\*,a d</sup>

<sup>a</sup>. School of Materials Science and Engineering, Shandong University of Technology, Zibo 255000, China.

<sup>b</sup>. College of nuclear equipment and nuclear engineering, Yantai University, Yantai 264000, China.

<sup>c</sup>. College of Materials Science and Engineering, Hunan University, Changsha 410082, China.

<sup>d</sup>. Shandong Industrial Ceramics Research & Design Institute Co., Ltd. No.128 Yumin Road, Zibo 255000, China.

\*E-mail: wang\_whhit@yeah.net; Wangfagang@sohu.com, g\_wen2016@163.com

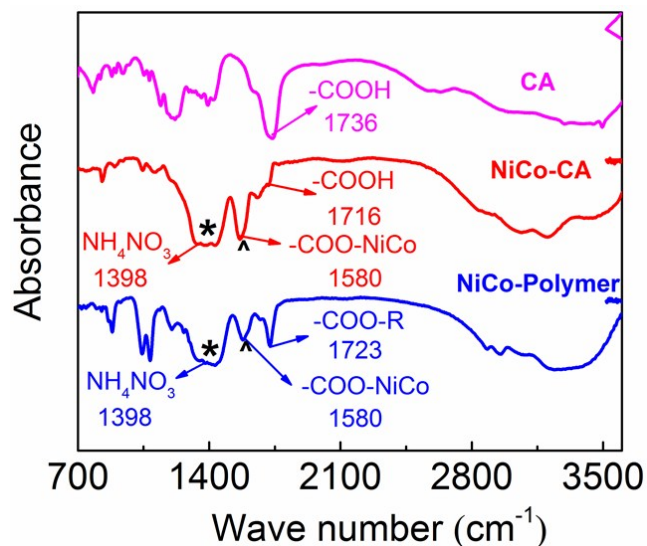


**Fig. S1** FTIR spectra of CA, NiCo-CA, and NiCo-polymer precursor.

In the FTIR spectrum of CA, the  $1736\text{ cm}^{-1}$  band is assigned to  $-\text{COOH}$  stretching vibration. It can be observed that in the FTIR spectrum of NiCo-polymer precursor, the typical vibrational band of  $-\text{COOH}$  is almost disappeared, indicating the occurrence of deprotonation. The two bands located at  $1580\text{ cm}^{-1}$  and  $1723\text{ cm}^{-1}$  should be attributed to  $-\text{COO-NiCo}$  stretching vibration and  $-\text{COO-R}$  stretching vibration, respectively, suggesting that there are interactions between  $\text{Ni}^{2+}$ ,  $\text{Co}^{2+}$  and  $-\text{COOH}$  in CA, as well as the esterification reaction between CA and EG. The FTIR results provide clear evidence of the formation of NiCo-polymer precursor. Besides, the band at  $1398\text{ cm}^{-1}$  indicates the formation of  $\text{NH}_4\text{NO}_3$ .

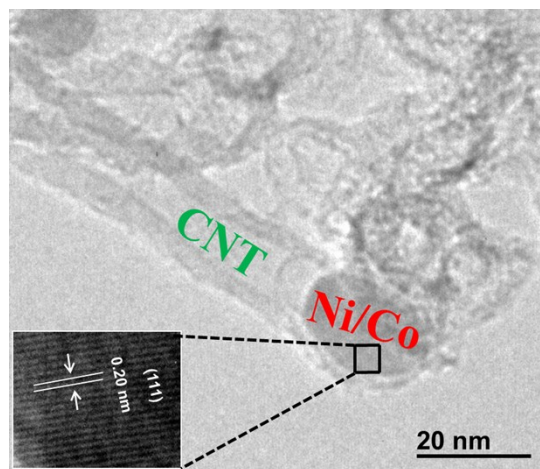


**Fig. S2** HRTEM image of N,O-CNTs before acid treatment.

Well defined lattice fringe of 0.20 nm should be assigned to the (111) plane of metallic NiCo nanoparticles.

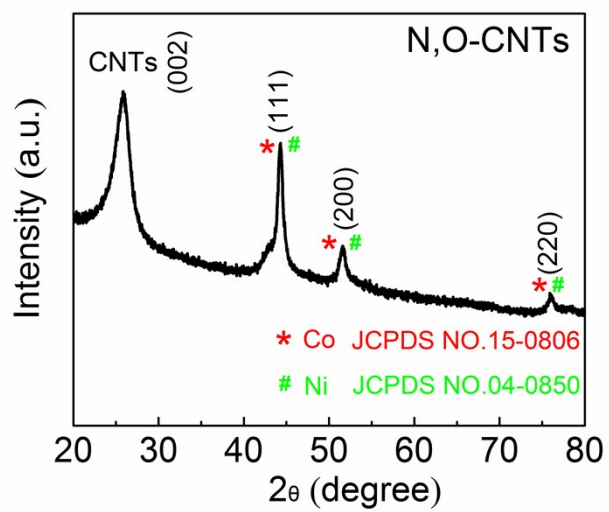


**Fig. S3** XRD pattern of the as-prepared N,O-CNTs.

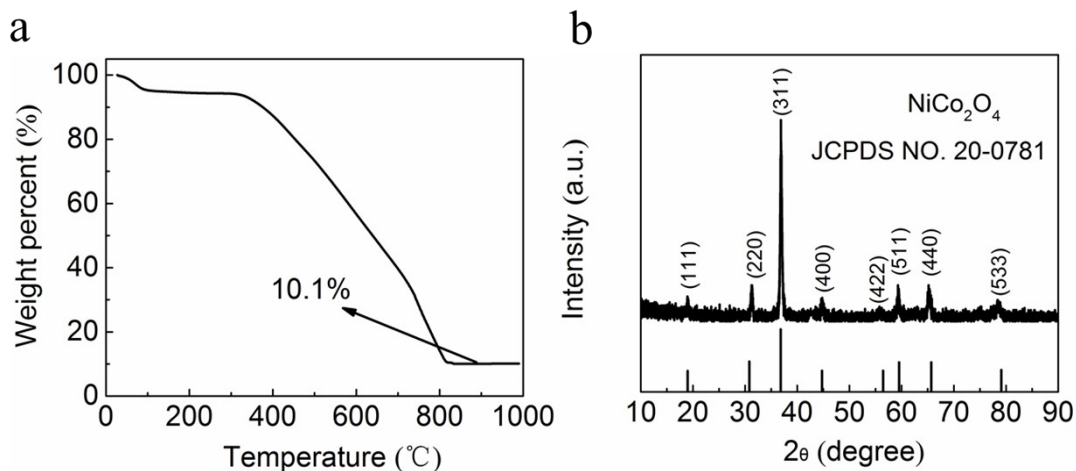


**Fig. S4** (a) TG analysis of N,O-CNTs after HCl treatment measured in air. (b) XRD pattern of the final product of N,O-CNTs after TG measurement in air.

To measure the amount of metal residual after HCl treatment, the TG analysis of N,O-CNTs after HCl treatment is carried out in air atmosphere (Fig. S4a). The result shows that the weight percent of final product after TG measurement is 10.1 wt%. Fig. S4b indicates that the final product after TG measurement is NiCo<sub>2</sub>O<sub>4</sub>. Thus, the weight percent of metal residual (NiCo) after HCl treatment is calculated as:

$$\frac{58.7 + 58.9 \times 2}{58.7 + 58.9 \times 2 + 16 \times 4} = 73.4\%$$

(1)

$$73.4\% \times 10.1\% = 7.4\% \tag{2}$$

Where 58.7 g mol<sup>-1</sup>, 58.9 g mol<sup>-1</sup> and 16 g mol<sup>-1</sup> are the molar weight of Ni, Co and O, respectively. The amount of metal residual after HCl treatment is ~7.4 wt%.

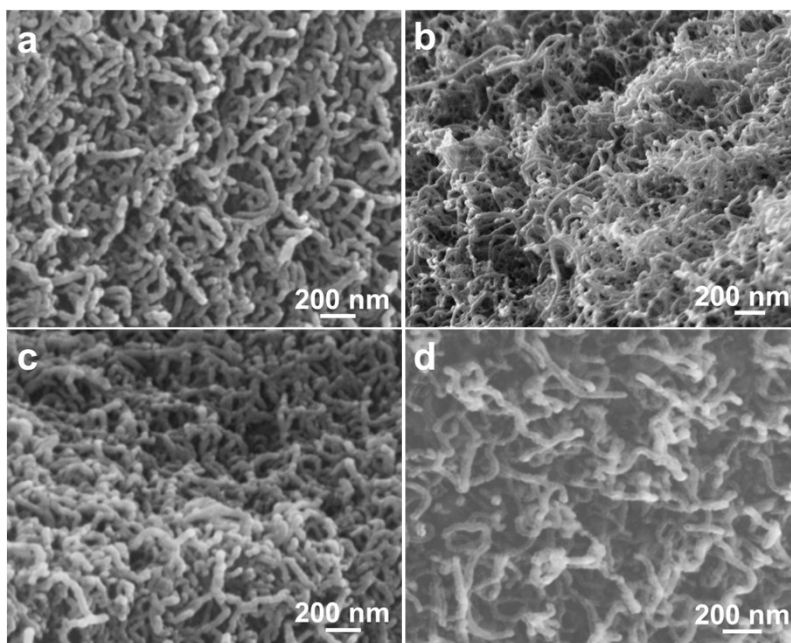


**Fig. S5** SEM images of the annealing products obtained from another four sets of experiments under the same conditions.

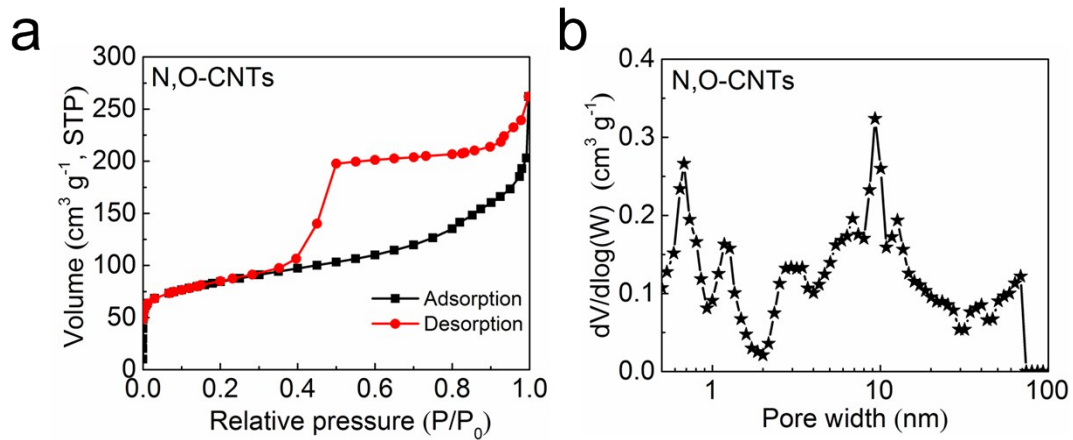


**Fig. S6** (a)  $\text{N}_2$  adsorption-desorption isotherms of N,O-CNTs and (b) the corresponding pore size distribution plot.

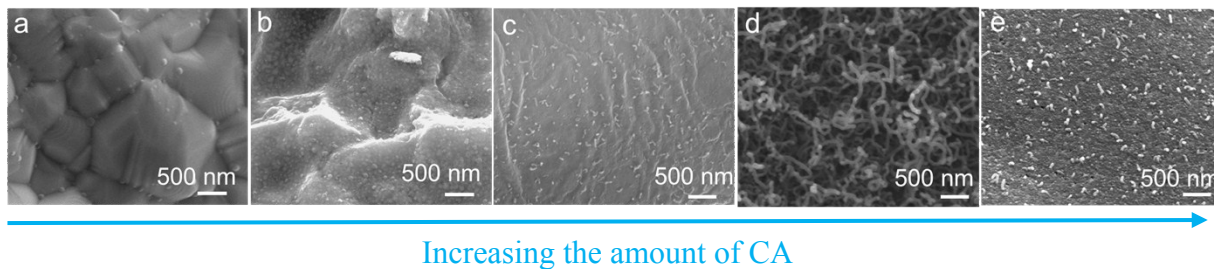


**Fig. S7** SEM images of the annealing products derived from the NiCo-polymer precursor with different molar ratios of metal ions/CA: (a) 1:0.5, (b) 1:1, (c) 1:1.6, (d) 1:3.2, and (e) 1:4.3.

In our MPM, typical product (N,O-CNTs) was obtained with 67.5 mmol metal ions and 216 mmol CA, corresponding to the metal ions/CA molar ratio of 1:3.2 (d). As a matter of fact, we started the experiment with metal ions/CA molar ratio of 1:0.5, which could only yield bulk NiCo alloys (a). However, a little amount of carbonaceous materials was observed on the surface of bulk NiCo alloys when the metal ions/CA molar ratio was 1:1 (b). When the metal ions/CA molar ratio reached 1:1.6, sparse and short CNTs were observed in the annealing products (c). Further increasing the amount of CA, we were able to obtain plenty of CNTs with regular shape and uniform sizes (d). However, when the metal ions/CA molar ratio is 1:4.3, the annealing products converted from interconnected high-density CNTs to large amount of amorphous carbon with sparse CNTs (e).

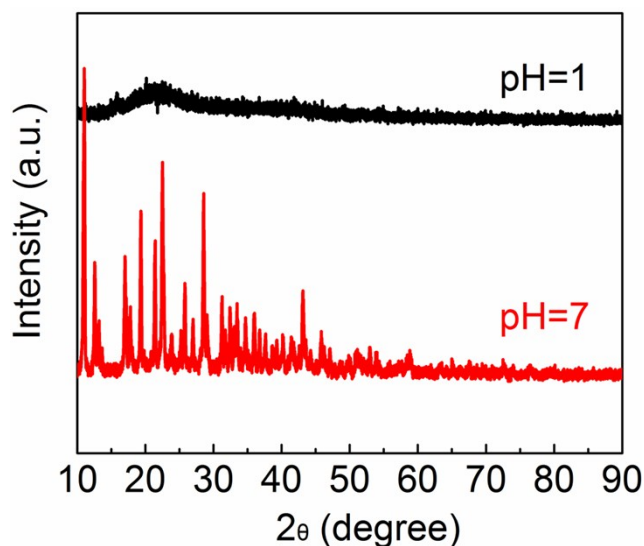


**Fig. S8** XRD patterns of the precursors obtained during the sol-gel process under different pH values.

When the pH value of the mixed solution is 1, the XRD pattern of the as-prepared precursor shows a broad shape without any diffraction peaks. However, when the pH value of the mixed solution is adjusted to 7 by adding  $\text{NH}_3 \cdot \text{H}_2\text{O}$ , the XRD pattern of the precursor exhibits a highly crystalline characteristic, which is similar to the metal-organic frameworks (MOFs).<sup>1,2</sup> Generally, MOFs are crystalline hybrid materials comprising coupling units (metal ions or metal-oxo units) coordinated by electron-donating organic ligands. Thus, the XRD results reveal the formation of NiCo-polymer frameworks in a neutral environment.

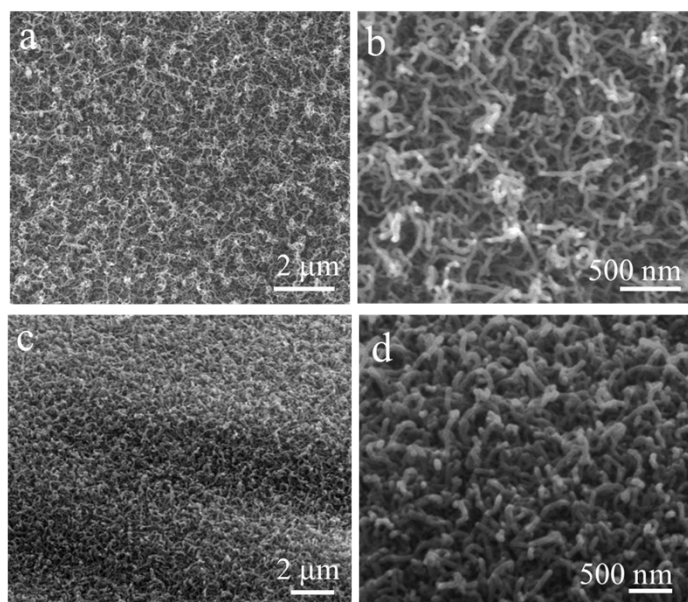


**Fig. S9** SEM images of the annealing products by adding only (a,b)  $\text{Co}(\text{NO}_3)_2 \cdot 6\text{H}_2\text{O}$  and (c,d)  $\text{Ni}(\text{NO}_3)_2 \cdot 6\text{H}_2\text{O}$  during the sol-gel process.

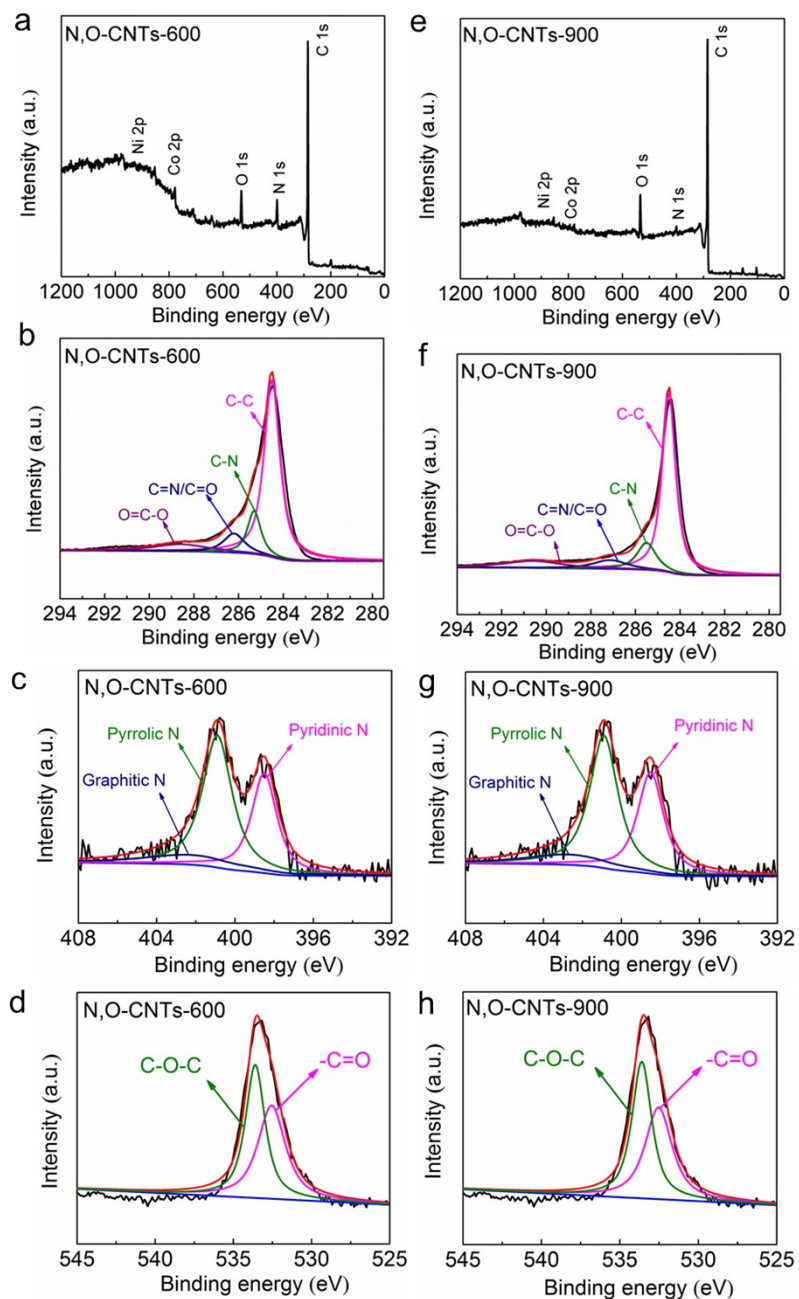


**Fig. S10** (a) Survey XPS spectrum, (b) C 1s spectrum, (c) N 1s spectrum, (d) O 1s spectrum of N,O-CNTs-600. (e) Survey XPS spectrum, (f) C 1s spectrum, (g) N 1s spectrum, (h) O 1s spectrum of N,O-CNTs-900.

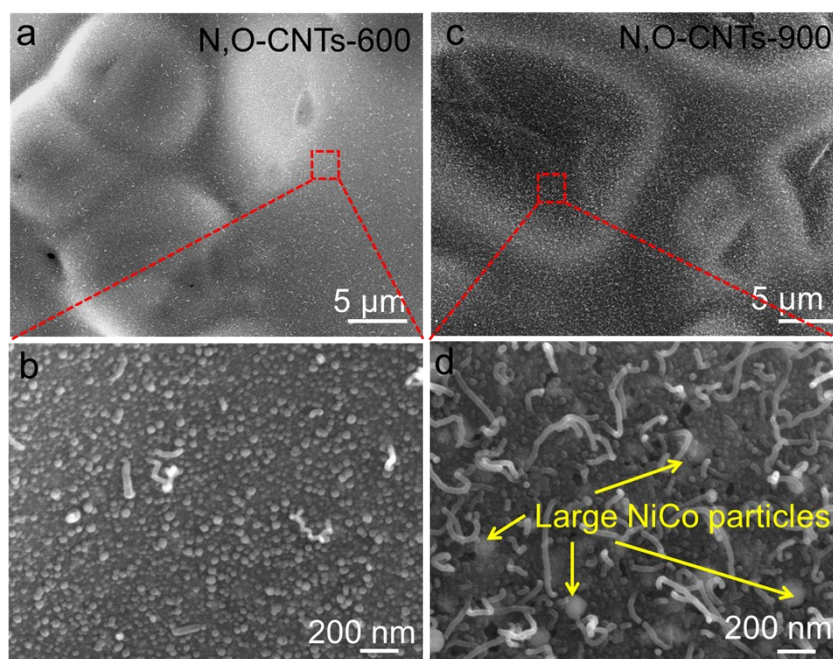


**Fig. S11** SEM images of (a, b) N,O-CNTs-600 and (c, d) N,O-CNTs-900 before the acid leaching treatment. The yellow arrows in (d) indicate the existence of large NiCo particles.

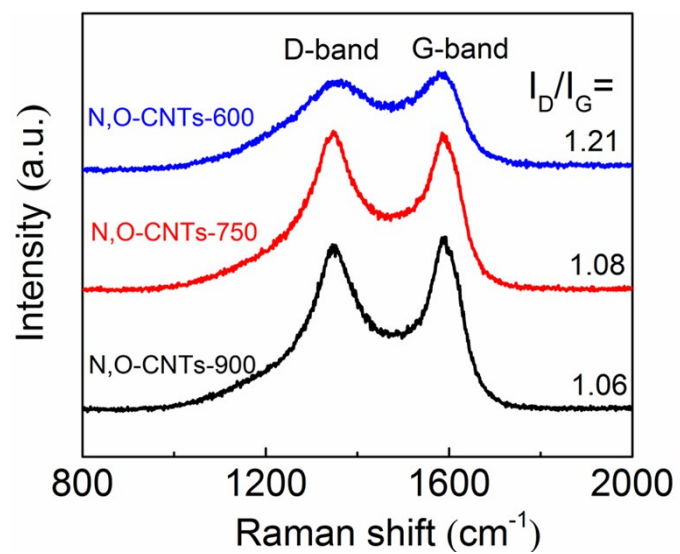


**Fig. S12** Raman spectra of N,O-CNTs-600, N,O-CNTs-750, and N,O-CNTs-900.

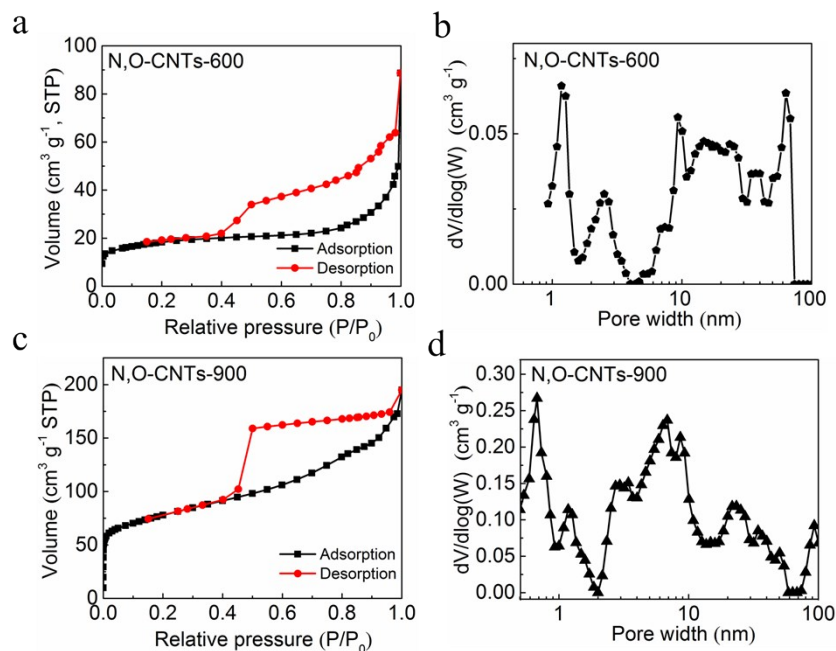


**Fig. S13** N<sub>2</sub> adsorption-desorption isotherms of (a) N,O-CNTs-600 and (c) N,O-CNTs-900 after the acid leaching treatment. Corresponding pore size distribution plots of (b) N,O-CNTs-600 and (d) N,O-CNTs-900.

The BET surface areas of N,O-CNTs-600 and N,O-CNTs-900 are 65.9 m<sup>2</sup> g<sup>-1</sup> and 279.0 m<sup>2</sup> g<sup>-1</sup>, respectively. The pore volumes of N,O-CNTs-600 and N,O-CNTs-900 are calculated as 0.14 cm<sup>3</sup> g<sup>-1</sup> and 0.27 cm<sup>3</sup> g<sup>-1</sup>, respectively.

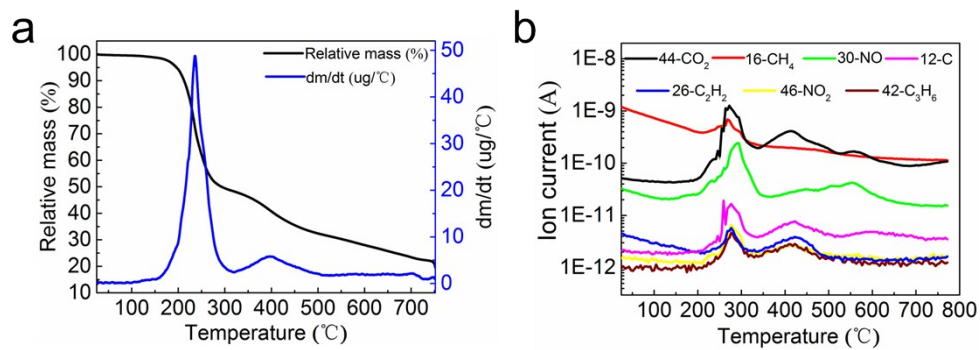


**Fig. S14** (a) TG-DTG curves of NiCo-polymer precursor measured in  $N_2$  atmosphere. (b) Corresponding MS curves of C,  $CH_4$ ,  $C_2H_2$ , NO,  $C_3H_6$ ,  $CO_2$ ,  $NO_2$ , respectively.

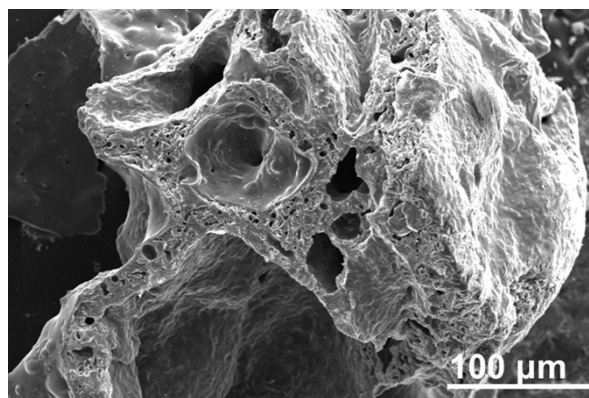


**Fig. S15** Low-magnification SEM image of the annealing product obtained by pyrolyzing the NiCo-polymer precursor at 750 °C with slow ramping rate of 2 °C min<sup>-1</sup>.

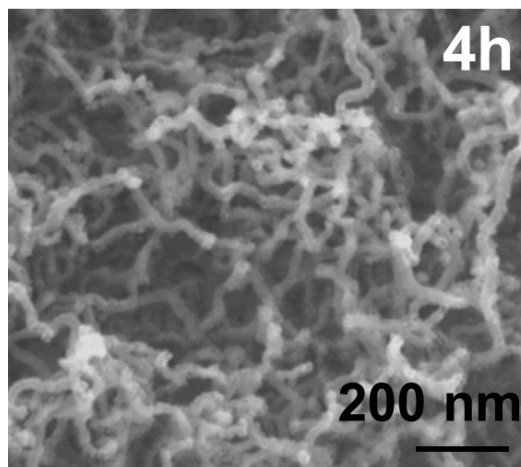


**Fig. S16** SEM image of the annealing product obtained at 750 °C for 4 h.

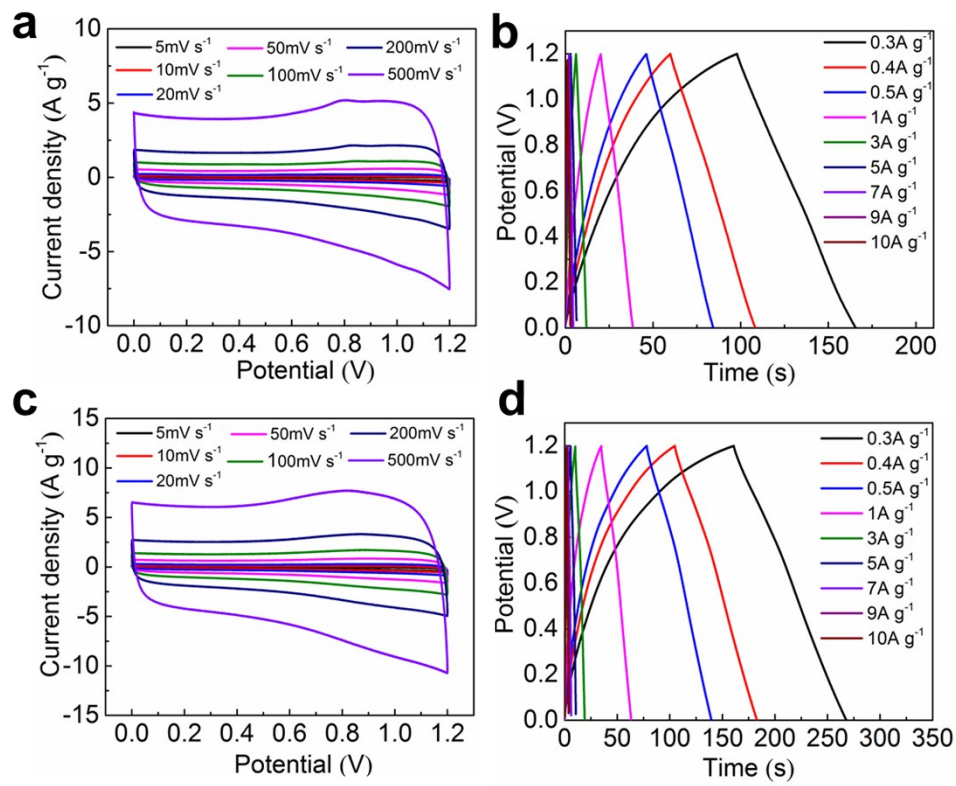


**Fig. S17** CV curves of (a) N,O-CNTs-600 and (c) N,O-CNTs-900. GCD profiles of (b) N,O-CNTs-600 and (d) N,O-CNTs-900.

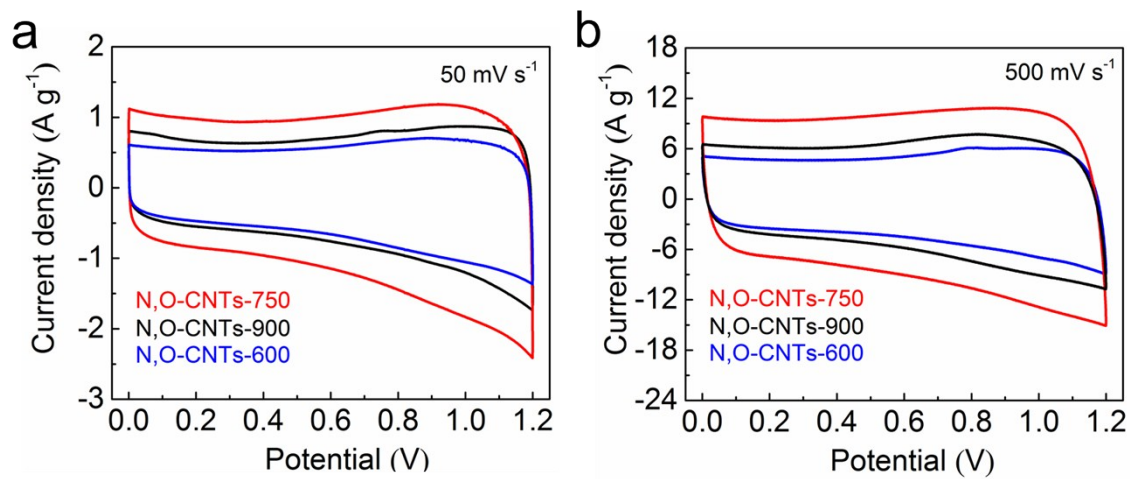


**Fig. S18** CV curves of N,O-CNTs-600, N,O-CNTs-750, and N,O-CNTs-900 based symmetric supercapacitors at (a) 50 mV s<sup>-1</sup> and (b) 500 mV s<sup>-1</sup>.

**Table S1.** Comparison of electrochemical performance of N,O-CNTs-750-SC and other CNTs-based supercapacitors in previous work.

Materials	Voltage range (V)	Electrolyte	Capacitance (Current density)	Capacity retention <sup>a</sup>	Ref
SWNTs	0–0.6	6.0 M KOH	40 F g <sup>-1</sup> (0.7A g <sup>-1</sup> )	□80% (2000)	3
N-CNTs/CF <sup>b</sup>	0–1.0	6.0 M KOH	133.1 F g <sup>-1</sup> (0.5 A g <sup>-1</sup> )	□95% (5000)	4
HCNTs	0–1.0	PVA/LiCl	125.7 F g <sup>-1</sup> (0.28mA cm <sup>-2</sup> )	□98%(15000)	5
PPy <sup>c</sup> @CNT	0–0.8	PVA/H <sub>2</sub> SO <sub>4</sub>	55.7 F g <sup>-1</sup> (0.2A g <sup>-1</sup> )	103% (2000)	6
PPy/9.6 wt% MCNT	0–0.6	1.0 M KCl	167.2 F g <sup>-1</sup> (0.5 mA cm <sup>-2</sup> )	83% (1000)	7
PPy/CNT	-0.8–0.5	1.0 M KCl	164 F g <sup>-1</sup> (0.2 A g <sup>-1</sup> )	55% (5000)	8
AC <sup>d</sup> /CNT/RGO <sup>e</sup>	0.01–3.0	1 M LiClO <sub>4</sub>	101 F g <sup>-1</sup> (0.2 A g <sup>-1</sup> )	75% (1000)	9
PPy/20wt% MCNT	0–0.6	1.0 M KCl	160 F g <sup>-1</sup> (0.5 mA cm <sup>-2</sup> )	85% (100)	10
MWNTs	0–1.0	6.0 M KOH	21 F g <sup>-1</sup> (500 mV s <sup>-1</sup> )		11
Vertically aligned MWNTs	0–1.0	1 M H <sub>2</sub> SO <sub>4</sub>	124 F g <sup>-1</sup> (20 mV s <sup>-1</sup> )	-	12
CNTs/PEDOT <sup>f</sup> sponge	-0.2–0.8	1 M H <sub>2</sub> SO <sub>4</sub>	147 F g <sup>-1</sup> (0.5 A g <sup>-1</sup> )	95% (3000)	13
GO <sup>g</sup> /PEDOT-CNT	-0.4–0.6	1.0 M KCl	91.6 F g <sup>-1</sup> (10 mV s <sup>-1</sup> )	97.5%(5000)	14
<b>N,O-CNTs-750</b>	<b>0–1.2</b>	<b>6.0 M KOH</b>	<b>162.5 F g<sup>-1</sup> (0.3A g<sup>-1</sup>)</b>	<b>97.6% (20000)</b>	<b>This work</b>

<sup>a</sup>) The capacity retention is calculated compared with the initial discharge capacity. <sup>b</sup>) CF: carbon foam. <sup>c</sup>) PPy: polypyrrole. <sup>d</sup>) AC: activated carbon. <sup>e</sup>) RGO: reduced graphene oxide, <sup>f</sup>) PEDOT: poly (3,4-ethylenedioxythiophene). <sup>g</sup>) GO: graphene oxide.

## References

- 1 F. Zheng, G. Xia, Y. Yang and Q. Chen, *Nanoscale*, 2015, **7**, 9637-9645.
- 2 D. Wang, W. Zhou, R. Zhang, X. Huang, J. Zeng, Y. Mao, C. Ding, J. Zhang, J. Liu and G. Wen, *J. Mater. Chem. A*, 2018, **6**, 2974-2983.
- 3 E. Frackowiak, K. Jurewicz, K. Szostak, S. Delpeux and F. Béguin, *Fuel Process. Technol.*, 2002, **77-78**, 213-219.
- 4 S. He, H. Hou and W. Chen, *J. Power Sources*, 2015, **280**, 678-686.
- 5 J. Cherusseri, R. Sharma and K.K. Kar, *Carbon*, 2016, **105**, 113-125.
- 6 R. Xu, F. Guo, X. Cui, L. Zhang, K. Wang and J. Wei, *J. Mater. Chem. A*, 2015, **3**, 22353-22360.
- 7 S. Paul, Y.-S. Lee, J.-A. Choi, Y. Kang and D.-W. Kim, *Bull. Korean Chem. Soc.*, 2010, **31** 1228-1232.
- 8 X. Lu, H. Dou, C. Yuan, S. Yang, L. Hao, F. Zhang, L. Shen, L. Zhang and X. Zhang, *J. Power Sources*, 2012, **197**, 319-324.
- 9 X. Li, Y. Tang, J. Song, W. Yang, M. Wang, C. Zhu, W. Zhao, J. Zheng and Y. Lin, *Carbon*, 2018, **129**, 236-244.
- 10 S. Paul, K.S. Choi, D.J. Lee, P. Sudhagar and Y.S. Kang, *Electrochim. Acta*, 2012, **78**, 649-655.
- 11 C. Du and N. Pan, *Nanotechnology*, 2006, **17**, 5314-5318.

- 12 E.O. Fedorovskaya, L.G. Bulusheva, A.G. Kurennya, I.P. Asanov, N.A. Rudina, K.O. Funtov, I.S. Lyubutin and A.V. Okotrub, *Electrochim. Acta*, 2014, **139**, 165-172.
- 13 X. He, W. Yang, X. Mao, L. Xu, Y. Zhou, Y. Chen, Y. Zhao, Y. Yang and J. Xu, *J. Power Sources*, 2018, **376**, 138-146.
- 14 H. Zhou, H.-J. Zhai and G. Han, *J. Power Sources*, 2016, **323**, 125-133.